Biochimica et Biophysica Acta, 973 (1989) 428–442
Elsevier

BBA 42956

EPR relaxation measurements of Photosystem II reaction centers: influence of S-state oxidation and temperature

R.G. Evelo [1], S. Styring [2,*], A.W. Rutherford [2] and A.J. Hoff [1]

[1] *Department of Biophysics, Huygens Laboratory of the State University, Leiden (The Netherlands) and* [2] *Service de Biophysique, Département de Biologie, CEN de Saclay, Gif-sur-Yvette (France)*

(Received 25 July 1988)
(Revised manuscript received 28 November 1988)

Key words: Manganese; Electron spin echo spectroscopy; Spin lattice relaxation time; Photosystem II; Oxygen evolution

The spin-lattice relaxation time of the EPR signal of the tyrosine radical D^+ has been measured with electron spin echo spectroscopy in the range 5–30 K in Photosystem II preparations with intact oxygen evolving complex (OEC). The charge storage state of the OEC was set by illumination with a series of flashes and monitored by measuring the multiline EPR signal of the S_2-state. The OEC was synchronized to 100% S_1 initial state by dark-adaptation and one preflash. Agreeing with previous work (De Groot, A., Plijter, J.J., Evelo, R., Babcock, G.T. and Hoff, A.J. (1986) Biochim. Biophys. Acta 848, 8–15), the spin-lattice relaxation curves were found to be bi-phasic. The average relaxation time $\bar{\tau}$ of each S-state was calculated from the data obtained for the 0–3 flash sample and the known S-state distribution. $\bar{\tau}$ was found to be maximal in the S_1-state. It decreased about 40% for the S_2-state, was essentially the same for the S_2- and the S_3-states and decreased again by about 55% for the S_0-state. These results are similar to those obtained earlier by cw EPR (Styring, S. and Rutherford, A.W. (1988) Biochemistry 27, 4915–4923). At 5 K the two exponentials describing the relaxation curves had characteristic times τ_f and τ_s that differed by an order of magnitude. Their amplitude was about equal, except for S_0 where the faster process predominated. At 20 K the characteristic time of both the fast and the slow process was reduced by a factor of about five; their amplitudes were again about equal. The observed relaxation times τ_f and τ_s were deconvoluted as a function of S-state by an approximate method. At 5 K it was found that τ_f was about twice as fast for S_0 and S_3 than for S_1 and S_2 (1.3 vs. 2.6 ms) and τ_s about twice as fast for S_0, S_2, S_3 than for S_1 (13.7–14.5 vs. 28.6 ms). The same trend was observed at higher temperatures. Interpreting the results with relaxation enhancement theory and integrating them with the results from cw EPR, NMR and EXAFS spectroscopy the following model for the OEC is presented. (i) To explain the biphasic relaxation of D^+ it is suggested that two Mn are close to D^+ at different distances, enhance the relaxation of D^+ and are not magnetically coupled. Their oxidation state differs by 1 unit, is probably Mn^{3+} and Mn^{4+}, and does not change during the $S_0 \rightarrow S_3$ sequence. It is postulated that at high temperature there is a charge resonance between the two Mn ions that is frozen out when cooling to cryogenic temperature. (ii) Two of the four Mn of the OEC form an antiferromagnetically coupled binuclear cluster in the oxidation state $Mn^{2+} \cdot Mn^{3+}$, $Mn^{3+} \cdot Mn^{3+}$, $Mn^{3+} \cdot Mn^{4+}$, $Mn^{3+} \cdot Mn^{4+}$ in the S_0, S_1, S_2 and S_3-state, respectively. (iii) From the temperature dependence of the relaxation of D^+ in the S_0-state, it is estimated that the distance between the Mn cluster and D^+ is 30–40 Å.

Introduction

The oxidation of water to molecular oxygen in plant photosynthesis is generally accepted to take place in a manganese-containing membrane-bound protein complex called the oxygen evolving Complex (OEC). The oxidizing equivalents produced by the photoreaction of Photosystem II (PS II) are stored by the OEC in a stepwise manner until four equivalents accumulate, water is oxidized in an apparently concerted reaction and dioxygen released. (Reviewed in Ref. 1.) The inter-

* Present address: Department of Biochemistry, Arrhenius Laboratory, University of Stockholm, S-10691 Stockholm, Sweden.

Abbreviations: Chl, chlorophyll; D^+, the radical that gives rise to EPR Signal II_{slow}; EPR, electron paramagnetic resonance; ESE, electron spin echo; EXAFS, extended X-ray absorption fine structure; Mes, 4-morpholineethanesulfonic acid; OEC, oxygen evolving complex; PPBQ, phenylparabenzoquinone; PS II, Photosystem II; XAES, X-ray absorption edge structure; Z, donor to the primary donor of Photosystem II.

Correspondence: A.J. Hoff, Department of Biophysics, Huygens Laboratory of the State University, P.O. Box 9504, 2300 RA Leiden, The Netherlands.

mediate oxidation states of the OEC are known as the S-states, S_0 to S_4. The chemical nature of the S-states has been the subject of numerous spectroscopic studies, all implicating manganese as the accumulator of oxidizing equivalents for some or all of the S-states.

The first direct evidence that one of the oxidation steps of the OEC involved Mn emerged from the observation of a multiline EPR signal at low temperatures in illuminated chloroplasts [2], which was similar to the EPR signal of a binuclear Mn model compound [3]. The dependence on the flash number and the temperature of photoinduction of the multiline signal suggested that it was correlated with the S_2-state [2,4–6]. Later work by several groups further characterized the multiline signal [1]. Another EPR signal at $g = 4.1$ is also associated with the S_2 state [4,7–10]. No EPR signals have been observed so far for the other S-states.

Further evidence for Mn chemistry being involved in S-state transitions comes from near IR [11,12] and UV measurements [12–17]. With these techniques flash number dependent absorption changes between 800 and 900 nm or 250 and 350 nm have been attributed to redox changes among the Mn ions.

Other evidence for the involvement of Mn in the OEC has come from Mn X-ray K-edge absorption and EXAFS spectroscopy (Refs. 18 and 19 and references therein). The EXAFS results suggested a μ-oxo-bridged Mn complex in both the S_1- and S_2-states, while a clear change in the K-edge inflection pointed to a change in the oxidation state of the Mn for the $S_1 \rightarrow S_2$ transition. No such change was observed for the $S_2 \rightarrow S_3$ transition [20]. Comparison with multi-nuclear Mn model clusters suggested that the oxidation states of the Mn in the OEC are Mn^{3+} or higher in the S_1- to S_3-states while S_0 is less well defined [20].

In addition to the above spectroscopic techniques, which yield more of less direct information on the Mn in the OEC, two indirect methods have been applied in which changes in magnetic relaxation are correlated with changes in the oxidation state of the OEC.

The proton NMR spin-lattice relaxation time of bulk water is influenced by the presence of paramagnetic impurities. Since the various oxidation states of Mn generally have quite different relaxation properties, the NMR relaxation of protons in bulk water in PS II preparation is expected to be sensitive to the oxidation state of Mn in the OEC. Indeed, Srinivasan and Sharp [21] showed that the proton relaxation rate R_1 was dependent on flash number. The changes were attributed to oxidation of Mn^{2+} to Mn^{3+} in the $S_0 \rightarrow S_1$ transition (decrease of R_1), Mn^{3+} to Mn^{4+} in the $S_1 \rightarrow S_2$ transition (increase of R_1) and $Mn^{4+} \rightarrow Mn^{2+}$ reduction in the $S_3 \rightarrow S_4 \rightarrow S_0$ transition (increase of R_1). No change was observed in the $S_2 \rightarrow S_3$ transition.

The OEC interacts chemically and magnetically with a component D, which in its oxidized form, D^+, gives rise to an EPR signal called Signal II [1]. D^+ was recently shown to be a tyrosyl-radical [22] that has been identified as Tyr-160 on the D_2 subunit [23,24]. D can donate an electron to S_2 or S_3 [25–28] while D^+ during dark adaptation accepts an electron from S_0 in a slow reaction [26]. The OEC is connected to the photochemical reaction center of PS II via a component Z which, when oxidized, has an EPR spectrum very similar to SII but with fast reduction kinetics. From the similar EPR spectra of Z^+ and D^+ and from extensions of the D_1/D_2 heterodimer concept it has been proposed that also Z^+ is a tyrosine radical, in this case on the D_1 protein [22–24].

The proximity of the OEC to Z^+ and D^+ suggests that their behavior must be susceptible to the functional integrity of the Mn cluster. Early cw EPR saturation studies of the EPR signals of Z^+ and D^+ indeed indicated that at least Z^+ and the Mn cluster interact magnetically [29–31]. Recently [32], the microwave power saturation at low temperatures of Signal II as a function of S-state was investigated in PS II-enriched membranes and it was shown that the half-saturation power, $P_{1/2}$, oscillated with flash number. At 8 K, $P_{1/2}$ was lowest in S_1 and highest in S_0. In S_2 and S_3, $P_{1/2}$ was similar and intermediate between $P_{1/2}$ in S_0 and S_1. From these data and the temperature dependence of $P_{1/2}$ in S_1 and S_2 it was concluded that the oscillation of $P_{1/2}$ originated from interactions between D^+ and the Mn cluster in the OEC. A model was suggested in which the changes in relaxation were due to interaction with a spin-coupled ($S = \frac{1}{2}$) $Mn^{2+} \cdot Mn^{3+}$ pair in S_0, a $Mn^{3+} \cdot Mn^{3+}$ pair ($S = 0$) in S_1 and a spin-coupled ($S = \frac{1}{2}$) $Mn^{3+} \cdot Mn^{4+}$ pair in both S_2 and S_3.

The relaxation of D^+ has also been studied by electron spin echo (ESE) spectroscopy and in a first paper it was shown that at 1.2 K D^+ in chloroplasts has a multiphasic spin-lattice relaxation, which depended on the illumination regime [33]. Part of the relaxation was due to a broad, about 1500 G-wide background signal [34], which probably was at least partly due to the integral representation of the (in the derivative representation) multiline signal of S_2 [2,35].

The relaxation behavior of D^+ at low temperature (5 K) was further investigated with ESE by De Groot et al. [36] who measured spin-lattice relaxation curves of PS II particles in samples prepared under various conditions of illumination, temperature and pH. It was reported that (i) in active oxygen-evolving particles the relaxation of D^+ was enhanced by a strongly relaxing species, which was associated with the OEC, (ii) the average relaxation time $\bar{\tau}$ of D^+ of active PS II preparations was decreased in the S_2-state compared to the S_0- and the S_1-states, and (iii) $\bar{\tau}$ was decreased even more in the S_3-state. These findings were interpreted as resulting from consecutive oxidation of Mn^{3+} to Mn^{4+} in the $S_0 \rightarrow S_1 \rightarrow S_2 \rightarrow S_3$ transitions.

In the above work, the various S-states were induced by raising the pH (S_0) or by illuminating dark-adapted samples at different temperatures (140, 200, 250 K). This procedure, however, does not completely inhibit formation of other than the desired S-state, so that likely some scrambling of S-states had occurred [37]. To obtain more precise information on the S-state dependence of the relaxation of D^+ and thus on the nature of the Mn cluster in the OEC in the various S states it is clearly desirable to measure the flash number dependence of the relaxation in samples in which the different S-states have been generated by consecutive flashes, starting with all OEC in one, well-defined S-state. The present communication presents the results of such an investigation, employing the dark adaptation/flash method of Refs. 32 and 37 to synchronize all OEC in the S_1-state.

A further objective of the present work is an investigation of the temperature dependence of the relaxation rate of D^+ in the four S-states. As will be shown below, in favorable cases one may observe a 'resonance' phenomenon when the spin-lattice relaxation of the Mn-cluster matches the EPR resonance frequency, which then allows conclusions to be drawn regarding the distance between the Mn-cluster or its components and D^+. Recently, it was found that the EPR saturation curves of D^+ showed a peculiar temperature dependence for the S_2-state suggestive of such a matching [32]. Since the ESE technique allows a more precise determination of the relaxation time than saturation measurements, it seemed worthwhile to reinvestigate the temperature dependence of the D^+ relaxation found in Ref. 32.

We find that in all S-states the relaxation curves are bi-exponential in the temperature range of 5–30 K. The average relaxation time, $\bar{\tau}$, of each sample measured at 5 K was deconvoluted to $\bar{\tau}$ values characteristic of the S_0- to S_3-states using the known S-state distribution of the 0–3 flash samples. It results that $\bar{\tau}$ of S_1 is slowest, $\bar{\tau}$ of S_2 and S_3 is almost equal and about 40% faster than $\bar{\tau}$ of S_1, and that $\bar{\tau}$ of S_0 is again 55% faster. Both for the two components of the bi-phasic relaxation similar results were obtained. The theory of relaxation enhancement by 3d transition metals is briefly introduced and used to construct a model of the OEC that incorporates the results of UV, NMR, EPR and X-ray spectroscopy. A preliminary account of this work was published in Ref. 38.

Materials and Methods

PS II-enriched membranes were prepared according to Ref. 39 with the modifications in Ref. 40. The membranes were stored at 77 K at 10 mg Chl per ml and were resuspended in 20 mM Mes buffer (pH 6.3) containing 0.4 M sucrose, 1 mM $CaCl_2$, 10 mM NaCl and 30% (v/v) ethylene glycol before use. PPBQ was added from a 20 mM solution in dimethylsulfoxide to a final concentration of 0.5 mM.

Sample preparation

For the EPR experiments PS II-enriched membranes at approx. 2 mg Chl per ml were transferred to calibrated EPR-tubes and incubated on ice in the dark for 2 h and at room temperature for 1 min. Thereafter a saturating preflash was given and the samples were allowed to equilibrate in total darkness at 20 °C for 9 min after which PPBQ was added as an exogenous acceptor. One minute thereafter the appropriate number of flashes (0–5) was given with a Nd-YAG frequency-doubled laser (15 ns, 300 mJ at 532 nm) and the samples were frozen within 2 s in an ethanol-solid CO_2 bath (200 K). The samples were immediately transferred to liquid nitrogen. The preflash treatment was considered necessary in these experiments, since it synchronizes the centers in the D^+S_1-state [26,37]. This also ensures that Signal II_s (D^+S_0) is fully converted to Signal II_u (D^+S_1) [25,26].

EPR spectroscopy

Cw EPR measurements were carried out in Saclay on a Bruker ESR 200D spectrometer. The instrument was equipped with an Oxford Instruments helium-flow cryostat and temperature controller. The amplitude of the S_2-state multiline signal was estimated from the added sum of low-field peaks as earlier described [26].

Pulsed EPR experiments were carried out in Leiden on a home-built ESE spectrometer [41], equipped with an Oxford Instruments helium-flow cryostat. The temperature was controlled with a home-built controller to within 0.5 K. Absolute temperatures are accurate to within 1 K. Electron spin echo field-swept spectra (where the magnetic susceptibility χ'' is displayed versus the magnetic field) were recorded using a two-pulse echo sequence with a spacing of τ_p ns between the two pulses. T_1 measurements were performed using a three-pulse sequence in which the two-pulse echo intensity is monitored as a function of the time, T, between the first (perturbing) pulse and the subsequent two-pulse echo sequence [34,36]. For most experiments a Space Microwave 1 kW microwave power amplifier was used, allowing a τ_p of 180 ns. For some control experiments the 20 W Varian TWT amplifier employed in Ref. 36 was used; τ_p was then 500 ns. The time resolution for T_1 measurements was better than 1 μs. The electron spin echo experiments were carried out at a repetition rate varying between 7 and 50 Hz depending on the temperature.

The average relaxation time, $\bar{\tau}$, defined as in Ref. 36, is the area above the relaxation curve (Fig. 3a). The

relaxation curves were fitted to a biexponential decay using the E04CGF fitting routine from the NAG library. To a good approximation all curves could be fitted with a bi-exponential.

Theory

To facilitate the discussion of the results the theory of relaxation enhancement will be briefly introduced. The relaxation (both spin-lattice or longitudinal and spin-spin or transversal) of a particular ensemble of electron spins in a magnetic field, designated here the relaxee, is influenced by the presence of other paramagnetic species, designated here the relaxer, through the action of fluctuating dipolar magnetic fields that are superimposed on the laboratory, static magnetic field. When the frequency of the dipolar fluctuations matches the frequency of transitions between the Zeeman levels of the spin system under consideration, transitions are induced that lead to a rapid establishment of equilibrium after a perturbing resonant microwave pulse. The frequency of dipolar fluctuations is governed by the correlation time of the relaxer, τ_c. Hence, the spin-lattice relaxation time, T_1, of the relaxee is a function of τ_c, the resonance frequency ω and of course of the magnetic moment of the relaxer. For a dilute spin system in the solid state, in which exchange interactions are negligible, the appropriate expression was derived by Solomon [42]:

$$\left(\frac{1}{T_1}\right)_d = \frac{2}{5}\frac{g^2\beta^2 S(S+1)\gamma_s^2\cdot\mu_0^2}{(4\pi)^2 R^6}\left[\frac{\tau_c}{1+\omega^2\tau_c^2}+\frac{4\tau_c}{1+4\omega^2\tau_c^2}\right] \tag{1}$$

where $(1/T_1)_d$ is the contribution to the spin-lattice relaxation of the relaxee resulting from the interaction with the relaxer, g is the electronic g-factor, β the electronic Bohr magneton, γ_s the electronic gyromagnetic ratio of the relaxer, S the total spin, τ_c its correlation time, $\mu_0 = 4\pi\cdot 10^{-7}$ the permeability in vacuum, ω the EPR resonance frequency corresponding to the laboratory magnetic field, and R the distance between relaxer and relaxee.

At low temperature we may take τ_c equal to the spin-lattice relaxation time T_{1R} of the relaxer (every spin flip induces a transient dipolar field). In the present case we assume that the relaxer is Mn, which is a 3d transition metal. Its relaxation is governed by the correlation time of the fluctuations of the crystal field potential due to its environment according to a relation derived by Bloembergen and Morgan [43] that is similar to Eqn. 1:

$$\frac{1}{T_{1R}} = B\left(\frac{\tau_v}{1+\omega^2\tau_v^2}+\frac{4\tau_v}{1+4\omega^2\tau_v^2}\right) \tag{2}$$

where B is a function of the ligand field splitting parameters. The correlation time, τ_v, is exponentially dependent on the temperature:

$$\tau_v = \tau_v^0\, e^{E_v/kT} \tag{3}$$

where E_v is an activation energy, k is Boltzmann's constant, and τ_v^0 a prefactor.

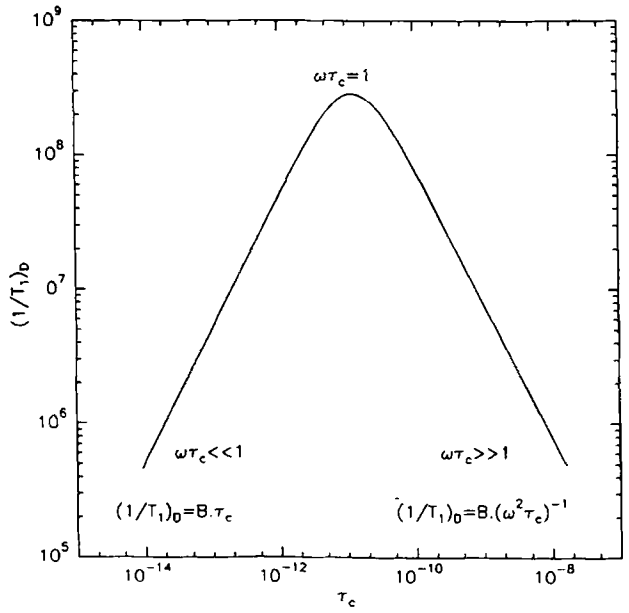

Fig. 1. Double logarithmic plot of the dipolar contribution to the relaxation of D^+, $(1/T_1)_d$, vs. τ_c ($= T_{1,Mn}$) for $\omega = 5\cdot 10^{10}$ s^{-1}, Eqn. 1. The approximate form of Eqn. 1 for the left and right hand branches of the plot are indicated. B is a proportionality constant.

Eqns. 1–3 are plotted in Fig. 1 in a double logarithmic plot. It is seen that the relaxation of the relaxee is maximally enhanced when $\omega\tau_c = 1$. As a function of temperature, the enhancement factor may increase, reach a maximum and then decrease again. The relaxer-induced relaxation is superimposed on the intrinsic spin-lattice relaxation of the relaxee, thus

$$\frac{1}{T_1} = \left(\frac{1}{T_1}\right)_i + \left(\frac{1}{T_1}\right)_d \tag{4}$$

In the present case, the relaxee is a tyrosine radical [22–24] whose intrinsic relaxation is governed by the so-called direct process, in which transitions are induced by modulations of environmental dipolar fields due to the lattice phonons. The temperature dependence of this process is given by Ref. 44:

$$\left(\frac{1}{T_1}\right)_i = a\coth\frac{\hbar\omega}{2kT} \tag{5a}$$

For $\hbar\omega \ll 2kT$, i.e., for X-band EPR and $T \geqslant 1$ K, this reduces to

$$\left(\frac{1}{T_1}\right)_i = a\cdot\frac{2k}{\hbar\omega}\cdot T = a'T, \tag{5b}$$

where a and a' are proportionality constants.

From Eqns. 1–5 it follows that the relaxation of D^+ will deviate most from a $(TT_1)^{-1} = a'$ behavior when $T_{1R} \approx \omega^{-1} \sim 2 \cdot 10^{-11}$ s. A curve of T_1^{-1} vs. T would then show an anomaly not unlike the feature found for the saturation curve for the S_2-state at about 20 K in Ref. 32. With T_{1R} known, Eqn. 1 then gives information on the distance R and on the total spin of the relaxer. When more than one relaxer is present the relaxation rate of the relaxee $1/T_1$ is then given by the sum of the intrinsic rate $(1/T_1)_i$ and the dipolar contributions $(1/T_1)_d$ of the individual relaxers, each with its own τ_v.

Results

Samples that were synchronized in the S_1-state by dark adaptation and preflash treatment [26,37] were subjected to 0–5 laser flashes at 300 K and rapidly frozen. The intensity of the S_2 multiline EPR signal as a function of the flash number is shown in Fig. 2. The flash pattern could be well simulated assuming 100% S_1-state for the 0 flash sample, 8% misses and no double hits. The resulting S-state distribution for the 0–5 flash samples is tabulated in Table I.

Flash number dependence

The spin-lattice relaxation of the EPR signal of D^+ of the 0–5 flash samples was subsequently measured with ESE spectroscopy, using the three-pulse technique. Fig. 3a–f shows the results obtained at 5 K. As found earlier [33–36], the recovery of the magnetization is non-exponential. The recovery trace can be represented

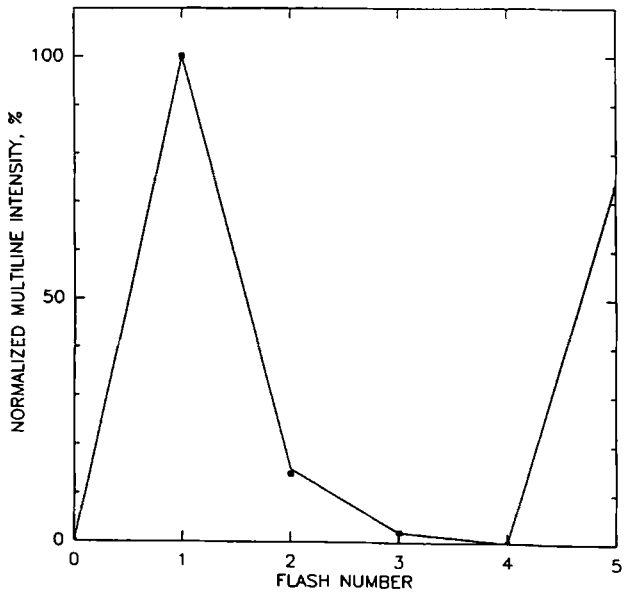

Fig. 2. The flash dependence of the intensity of the S_2-state multiline EPR signal in synchronized PS II-enriched membranes (■), experimental; (———) simulation assuming 100% S_1-state before the flashes, 8% misses and no double hits.

TABLE I

The expected S-state distribution in percent after 0–5 flashes calculated assuming 100% S_1 from the start, 8% misses and no double hits

The samples were synchronized as described in the Materials and Methods section.

No. flashes	S_1	S_2	S_3	S_0
0	100	–	–	–
1	8	92	–	–
2	–	15	85	–
3	–	2	20	78
4	72	–	3	25
5	29	66	–	5

by

$$f(t) = 1 - \sum c_i e_i^{-t/\tau_i}, \quad \text{with} \quad \sum c_i = 1 \tag{6a}$$

The area I above the curve (shaded in Fig. 3a), given by

$$I = \int_0^\infty f(t)\, dt = -\sum_i c_i \tau_i = -\bar{\tau} \tag{6b}$$

defines a weight-averaged relaxation time $\bar{\tau}$. Clearly, $\bar{\tau}$ depends strongly on the flash number, being maximal for the 0-flash sample (100% S_1), decreasing stepwise for the first three flashes to about one third of the 0-flash sample, and then steeply increasing for the 4-flash sample, in which the S-state is again predominantly S_1.

The relaxation traces could be well fitted with bi-exponential recoveries, indicated by the solid lines in Fig. 3. Fig. 3 also shows the residuals (the differences between the data points and the fit). Table II shows the fit parameters and the average recovery time $\bar{\tau}$ for the six samples. The fits show that the recovery is characterized by a fast and a slow contribution, the characteristic times of which differ by an order of magnitude. The two contributions are present in about equal proportions, except in the 3-flash sample where the amplitude of the fast contribution seems to be somewhat enhanced. A fit of the 3-flash recovery trace with fixed, equal, amplitudes and free recovery times was not acceptable. The characteristic times, τ_f and τ_s, for the fast and slow contributions to the recovery, respectively, were flash number dependent, τ_f being smaller than the 0-flash value for the 2- and 3-flash samples and τ_s being smaller than the 0-flash τ_s for the 1-, 2-, 3- and 4-flash samples.

The relaxation measurements were repeated at a number of temperatures in the 5–30 K range. The results for 20 K are shown in Fig. 3(g–i) and in Table II. Again the recovery traces are well fit with bi-exponentials. In Fig. 4 it is seen that the flash depence of $\bar{\tau}^{-1}$ persists up to 30 K, and may even get somewhat more pronounced. For all six samples the relative amplitude of the faster process seems to be enhanced relative to the 5 K results.

The average relaxation time $\bar{\tau}_i$ of each S_i state can be calculated from the data in Tables I and II, using the relation $F(t) = \Sigma_j f_j(t)$, $j = 0-3$, where $f_j(t)$ represents the recovery curve of the S_j state (see Appendix A) and the $F(t)$ values are the recovery curves of the 0- to 3-flash samples. For the data taken at 5 and 20 K the results, together with the predicted and experimental values for the 4- and 5-flash sample, are collected in Table III. A similar excercise is possible only approximately for the decomposition of the recovery traces in a fast and a slow component (see Appendix A). The (approximate) values of τ_f and τ_s for the S_0-, S_2- and S_3-states are also shown in Table III. As a control, the average $\bar{\tau}$ was computed for the calculated τ_f, τ_s and a_1, a_2 (the c_{kj} and τ_{kj}, $j = 0-3$, $k = 1$ and 2 from the Appendix) for each S-state and for the 4- and 5-flash sample. From Table III is seen that the agreement is quite good, which serves as a justification a posteriori that the approximations involved in the calculation of the τ_f and τ_s values of each S-state did not lead to serious errors.

Table III shows that at 5 and 20 K the average decay time $\bar{\tau}_j$ depends strongly on the S-state. The S_1-state, the starting point of our flash series, has by far the slowest relaxation. The relaxation time drops by about 40% in the S_2-state, and remains about the same when the OEC advances to the S_3-state. The reductive transition to the S_0-state again lowers the relaxation time by more than 50%. In terms of relaxation rates, the S_0-state shows the largest enhancement, which is dramatically lowered (by a factor of more than 3) for the S_1-state. The S_2- and S_3-states show about the same, intermediate relaxation enhancement. Thus, the S_0-state is the strongest relaxer, the S_2- and S_3- states are intermediate relaxers with about equal relaxation enhancement, and the S_1-state is only a weak relaxer. This agrees quite nicely with the cw EPR saturation data of Ref. 33 and validates the use of the saturation method as a qualitative tool to study the relaxation behavior of the Mn cluster of the OEC. For the decomposition in τ_s and τ_f of the individual S-states, we find that at 5 K τ_f is significantly higher in the S_1- and S_2-states than in the S_3- and S_0-states, its value in the S_2-state being rather different from that in S_3. τ_s follows closely the pattern set by the $\bar{\tau}_j$ for the S_1–S_3 states. The fast $\bar{\tau}$ in the S_0-state seems to be caused by a much larger contribution of the fast relaxing species, τ_s in S_0 being only slightly lower than that in S_2 and S_3. The above pattern is largely reproduced for the 20 K data.

Temperature dependence

The relaxation recovery curves of all flash samples were measured at a number of temperatures in the range 5–30 K. The inverse of the average relaxation time $\bar{\tau}$ as defined before is plotted as a function of temperature in Fig. 5. The 0-flash sample (state S_1) shows an almost linear dependence of the average relaxation rate on temperature. The 1- and 2-flash samples (predominant states S_2 and S_3, respectively) show a somewhat enhanced relaxation around 20 K. This enhancement is dramatically increased for the 3-flash, S_0-state sample.

Discussion

Flash dependence

The results in Table III and Fig. 4 clearly indicate that the average relaxation time $\bar{\tau}$ greatly depends on the S-state. At 5 K the relaxation in the S_2- and S_3-states is about 40%, and in the S_0-state about 70% faster than in the S_1-state. This pattern is preserved at higher temperatures, up to 20 K. Thus, between 5 and 20 K the relaxation in S_1 is slowest, that in S_2 and S_3 is about the same, while in S_0 the relaxation is by far the fastest. In

TABLE II

Spin-lattice relaxation of D^+ (Signal II) in PS II-enriched membranes exposed to 0–5 flashes

Flash	Predominant S-state	T (K)	Bi-exponential fit				$\bar{\tau}$ [a]
			weight (%)	lifetime (ms)	weight (%)	lifetime (ms)	
0	S_1	5	51.4	2.6	48.6	28.6	13.8
1	S_2	5	54.1	2.5	45.9	14.9	9.0
2	S_3	5	54.2	1.3	45.8	14.5	7.8
3	S_0	5	74.5	1.4	25.5	14.0	5.0
4	S_1	5	59.6	1.7	40.4	17.1	9.3
5	S_2	5	52.7	1.9	47.3	15.2	9.6
0	S_1	20	40.6	0.6	59.4	5.2	2.9
1	S_2	20	41.6	0.3	58.4	3.1	1.7
2	S_3	20	64.2	0.3	35.8	3.7	1.5
3	S_0	20	49.5	0.3	50.5	1.7	0.73
4	S_1	20	55.7	0.6	44.3	3.9	2.0
5	S_2	20	60.7	0.5	39.3	5.9	2.6

[a] Experimental value measured as the shaded area in normalized plots as in Fig. 3a.

view of the bi-exponentiality of the relaxation in the S_1-state, even in this slowly relaxing state there must still be a sizeable dipolar contribution to the relaxation of D^+. The nature of this contribution is discussed in the next section.

Two relaxation processes

In all samples investigated in this and earlier work [33–36], the relaxation of D^+ is bi-exponential, the two exponentials having about equal amplitudes and characteristic times that differ by about an order of magnitude. In order to investigate spin diffusion as a possible cause of the fast relaxation process [46], relaxation measurements were performed with two different pulse widths for the $\pi/2$ pulse, viz. 20 and 60 ns, keeping the Q-factor of the EPR cavity the same. Therefore, the relative magnitude of the pulsed H_1 microwave fields and consequently the initial width of the 'holes' (the ensembles of spin packages affected by the microwave fields) were different by a factor of $\sqrt{3}$. The relative amplitude of a spin-diffusion induced relaxation process depends strongly on the initial hole width [47]. We found that the relaxation times τ_1 and τ_2 and the relative amplitude of the bi-exponential decay were identical for the 20 and 60 ns pulses to within our measuring accuracy (1.5–3.0%). Thus we conclude that the contribution of spin diffusion to the fast component is negligible.

If one relaxee interacts with more than one relaxer of different relaxation enhancement, the relaxee's relaxation is still exponential with a characteristic rate that is the sum of the individual enhanced relaxation rates and its own intrinsic rate. In other words, an OEC containing four Mn in different magnetic states and with different distances to D^+ would still act as one, averaged, relaxer *. The non-exponentiality of the relaxa-

* To appreciate this point it is helpful to think of relaxation as the emptying of a bucket of water (the relaxee) by a series of holes of different size (the relaxers).

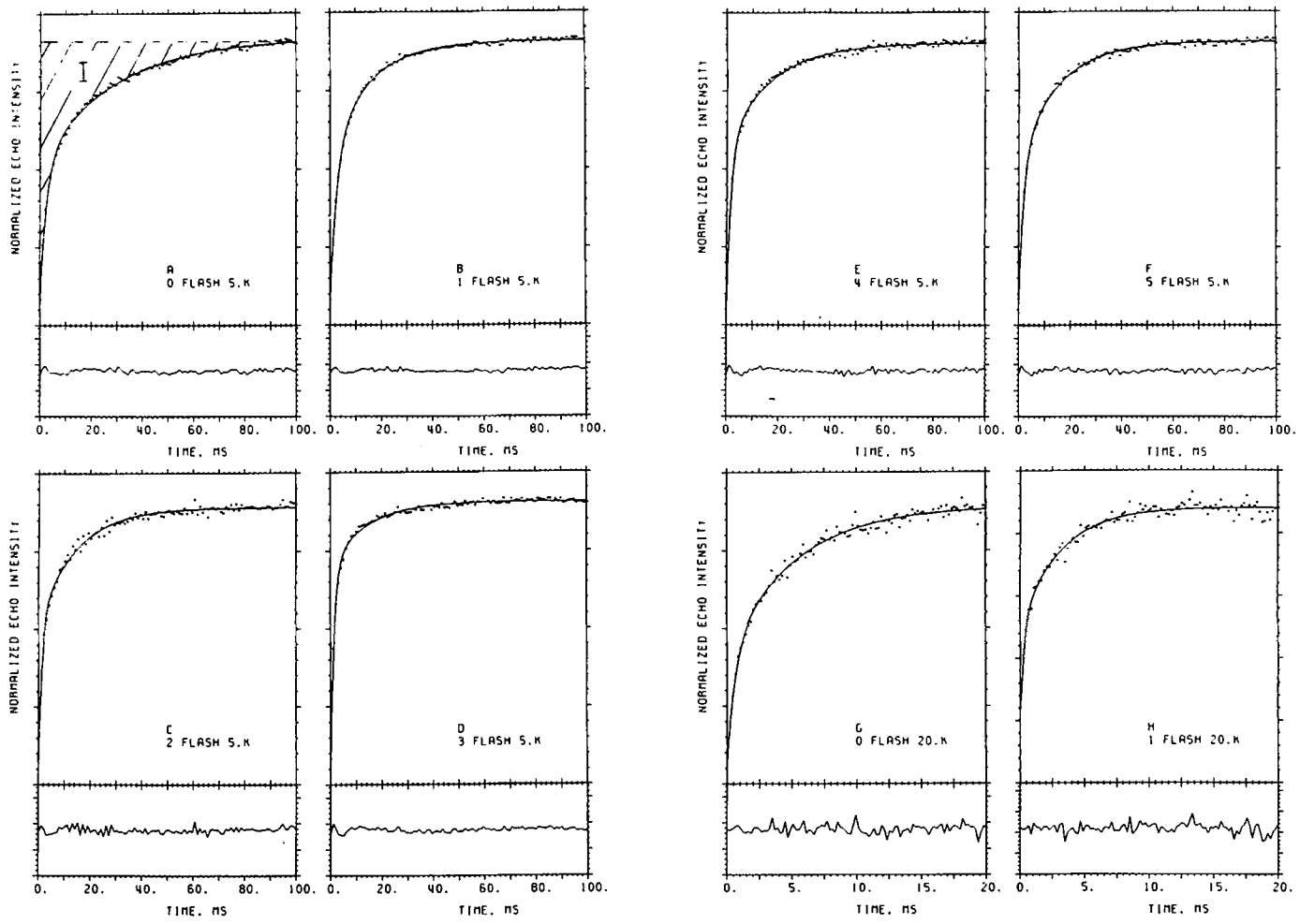

Fig. 3. The recovery of the population inversion in the 0–5-flash samples measured at 5 K (a–f) and 20 K (g–l) with a 3-pulse echo sequence. $\pi - \frac{1}{2}\pi - \pi$, with variable spacing between the first π and the $\frac{1}{2}\pi$ pulse and 280 ns delay between the $\frac{1}{2}\pi$ and second π pulse. Smooth drawn lines are bi-exponential fits; the residuals (as defined in the Materials and Methods section) are shown at the bottom of each panel. The hatched area in (a) defines the average relaxation time $\bar{\tau}$ as explained in the text.

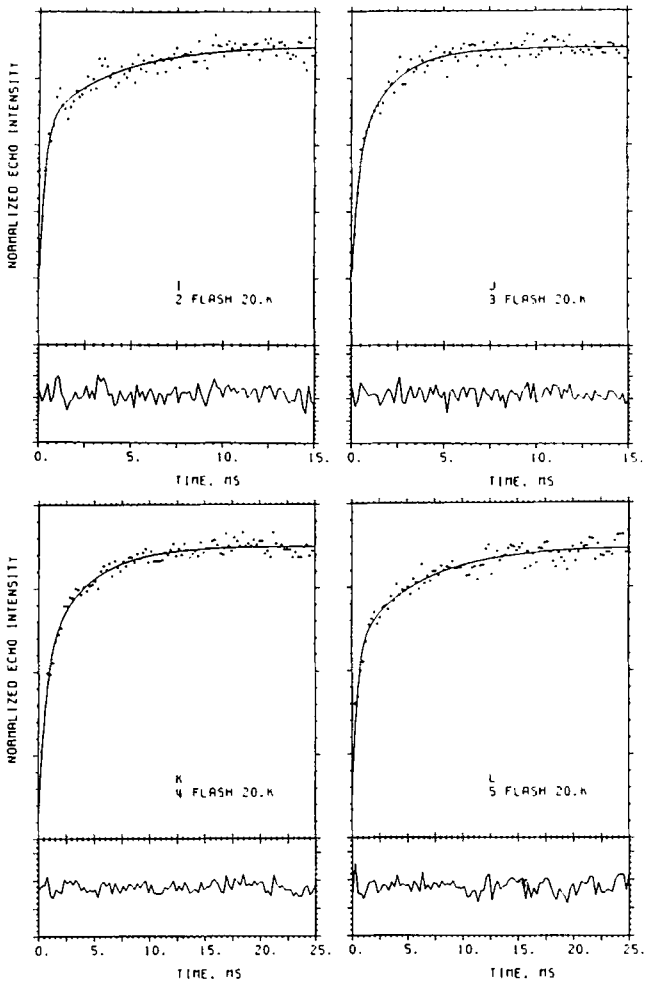

Fig. 3 (continued).

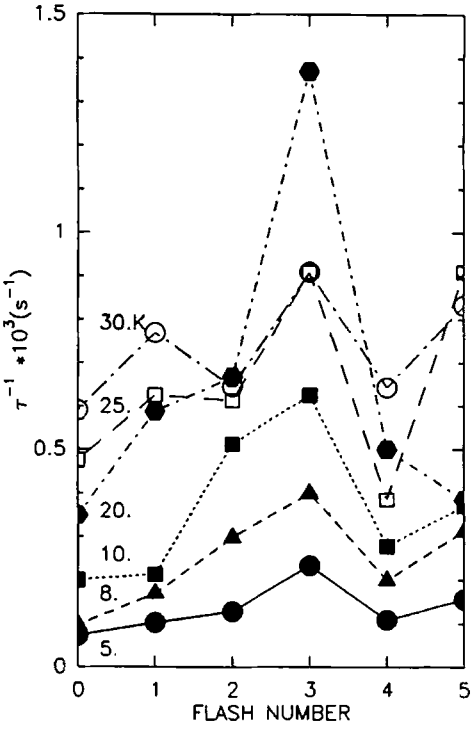

Fig. 4. Flash number dependence of the average relaxation rate $\bar{\tau}^{-1}$ at temperatures 5–30 K as indicated.

tion must therefore originate from (at least) two populations of D^+ (a bi-modal heterogeneity of the D^+-OEC system).

So-called β-centers as source for the heterogeneity can be ruled out since they are not present to any significant extent in PS II-enriched membranes [48].

TABLE III

Calculated relaxation times in ms and relative amplitudes for the two relaxation processes in the individual S-states and of the 4- and 5-flash sample at 5 and 20 K

The calculations were carried out as described in Appendix A.

S-state	a_f [a]	τ_f [a]	a_s [a]	τ_s [a]	$\bar{\tau}$ [b]	$\bar{\tau}$ calc [c]
Temperature 5 K						
S_1	0.51	2.6	0.49	28.6	13.8	
S_2	0.55	2.5	0.45	14.3	8.6	9.2
S_3	0.54	1.2	0.46	14.5	8.7	7.3
S_0	0.80	1.4	0.20	13.7	4.0	3.9
4-flash [d]	0.60	1.8	0.40	24.1	11.2	10.8
5-flash [d]	0.53	2.3	0.47	17.7	9.9	9.7
Temperature 20 K						
S_1	0.41	0.60	0.59	5.2	3.3	
S_2	0.42	0.29	0.58	3.0	1.9	1.9
S_3	0.68	0.30	0.32	4.0	1.5	1.5
S_0	0.45	0.30	0.55	1.6	1.0	1.0
4-flash [d]	0.42	0.46	0.58	3.3	2.1	2.1
5-flash [d]	0.42	0.34	0.58	3.3	2.6	2.1

[a] Calculated with Eqn. A-9 and A-10 from the data of Table II.
[b] Calculated with Eqn. A-5 from the $\bar{\tau}$ values of Table II.
[c] Calculated with a_f, τ_f, a_s and τ_s from this table.
[d] Calculated with the above values for S_0–S_3 and the S-state distribution of Table I.

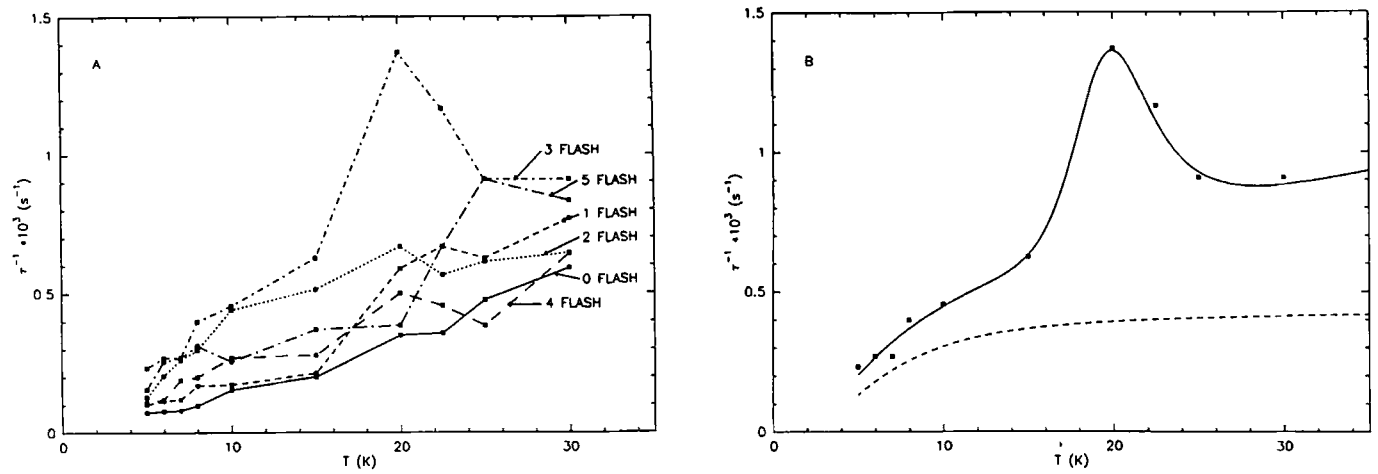

Fig. 5. (A) Temperature dependence of the average relaxation rate $\bar{\tau}^{-1}$ in the 0–5-flash samples. (B) (■) Data of the 3-flash sample, (———) a fit to the temperature dependence of $\bar{\tau}^{-1}$ of the 3-flash sample by the relation $\bar{\tau}^{-1} = a'T + c_1 f_1(\tau_v) + c_2 f_2(\tau_v')$. The term $a'T$ represents the direct process with $a' = 14.3\ K^{-1}\cdot s^{-1}$; $c_1 f_1(\tau_v)$ represents a weakly temperature-dependent dipolar contribution (dashed line) with $\omega T_{1,Mn} \gg 1$ and parameters ω, b, B and τ_v as defined in Eqns. B-1–B-3: $\omega = 5\cdot 10^{10}\ s^{-1}$, $bB = 1.75\cdot 10^{34}\ s^{-4}$, $\tau_v = 1.2\cdot 10^{-11}\ e^{10/T}$ s; $c_2 f_2(\tau_v')$ represents a strongly temperature-dependent dipolar contribution with $b = 2.43\cdot 10^{13}\ s^{-2}$, $B = 2\cdot 10^{25}\ s^{-2}$, $\tau_v' = 5.5\cdot 10^{-12}\ e^{210/T}$ s.

The earlier reported heterogeneity in Signal II_s [25] is due to different reactivity between D^+ and the S-states and not to structural heterogeneity. The phenomenon is explained in detail in Ref. 26.

S-state heterogeneity as a possible cause for the bi-phasic relaxation behaviour can also be ruled out. It is known that the multiline signal inducible by 200 K illumination corresponds to approximately one spin per reaction center [10]. The maximal amplitude of the multiline signal of the one-flash sample was 90–95% of that of a sample illuminated at 200 K (data not shown). Thus, maximally 10% of the reaction centers do not contribute to the S-state oscillations, in keeping with our miss parameter of 8% in the simulation of the multiline amplitude (Fig. 2). Note also that the presence of ethylene glycol in the sample results in the conversion of the $g = 4.1$ signal to the multiline signal [9].

In principle, a heterogeneity of D^+ could arise from two populations of D^+ with different distances to the OEC [38]. The fact, however, that there is some flash dependence of the relative amplitudes of the fast and slow relaxation processes, notably in the S_0-state, and a clear temperature dependence (Table II) makes this possibility in our view less likely.

Another explanation is that the bi-exponentiality is due to two, magnetically non- or only weakly coupled Mn ions that differ in relaxation time, for example a Mn^{4+} (a fast relaxer) and a Mn^{2+} or low spin Mn^{3+} (slow relaxers). If one Mn is appreciably closer to D^+ than the other Mn, and if there is a charge resonance equilibrium between the two Mn ions that is frozen in at low temperatures, one would have two populations of D^+ with different relaxation rates, the relative concentration of which is dependent on the equilibrium constant of the charge resonance process. In the complete OEC, two more Mn are present. Changes in the magnetization of these two Mn would then both enhance the slow and the fast relaxation processes, in agreement with the observations.

We note that a Tris-EDTA-washed preparation, which has an incomplete, inactivated OEC, still shows a bi-exponential relaxation, with amplitudes and rates that are close to those found in the 0-flash samples (100% S_1) [36]. In the current view Tris-EDTA washing removes 2 or 3 to 4 Mn ions [49–51]. It is likely that the Tris-EDTA treatment produces a heterogeneous material that will give several exponentials for the spin-lattice relaxation of D^+. Therefore, we cannot compare our present results on intact, fully active O_2-evolving particles with those obtained in Ref. 36 on Tris-treated, inactivated samples.

Temperature dependence

The temperature dependence of the relaxation rate of D^+ follows by combining Eqns. 2–4 and Eqn. 5b. For simplicity we lump the dipolar contribution to one average rate $(1/T_1)_d^{-1}$. The temperature dependence of the dipolar contribution is then given by Eqns. 2 and 3. Little is known of τ_v but we can discern several limiting cases for the temperture dependence of $(1/T_1)_{D^+}$, all of which lead in the high temperature limit asymptotically to a linear dependence as in Eqn. 5b (see Appendix B). A special case arises when $T_{1,Mn}$ becomes close to ω^{-1}. We then obtain a kind of a resonance phenomenon: $(T_{1,Mn})^{-1}$ rises rapidly with increasing temperature, and then falls off again.

Considering now Fig. 5A, we see that $(\bar{\tau})^{-1}$ of the 0-flash sample depends approximately linearly on temperature. This means that we are in one of the limiting cases of Appendix B: a dominant direct process with

relatively small dipolar enhancement. The relaxation of the 1- and 2-flash samples is clearly appreciably enhanced over that of the 0-flash sample, yet if there is a temperature 'resonance' it is only small. Thus, the dipolar contribution to the relaxation is stronger than the direct process but either $\omega T_{1,Mn} \gg 1$ or $\omega T_{1,Mn} \ll 1$ so that we are far from a resonance condition. We note that in the microwave power saturation studies of Ref. 32 there is a somewhat stronger enhancement of $P_{1/2}$ for the 1- and 2-flash samples around 20 K than that of $(\bar{\tau})^{-1}$ in Fig. 5A. This is presumably due to the spin-spin relaxation time T_2, which influences $P_{1/2}$ in a similar manner as $\bar{\tau}$, and which decreases rather rapidly with temperature in this region (data not shown).

We attribute the overall increase in relaxation of the 1- and 2-flash sample over that of the 0-flash sample to oxidation of the Mn in the OEC. Since the S_2-state (1-flash sample) is most probably a $S = \frac{1}{2}$, antiferromagnetically coupled binuclear Mn cluster, it is reasonable to assign the enhancement of the 1-flash sample to the formation of this paramagnetic state. The temperature dependence of the relaxation of the 2-flash sample (S_3-state) is not much different from that of the 1-flash sample. In view also of the fact that at the low end of the temperature range studied, where $\bar{\tau}$ is determined most accurately, the relaxation is practically the same for the 1- and 2-flash samples, we believe that also in the latter sample (predominant S_3-state) the $S = \frac{1}{2}$ cluster is still present (see also below).

The temperature dependence of the 3-flash sample (predominant S_0-state) is significantly different from that of the 0–2 flash samples. There is a pronounced increase at 20 K followed by a drop at higher temperatures (Fig. 5A, B). This behavior is typical for a temperature 'resonance' as discussed above. The smooth line in Fig. 5B represents a simulation using Eqns. 1–4 and 5b with two dipolar interactions, one with a weak temperature dependence (dashed line in Fig. 5B) and one with a temperature dependence peaking at 20 K. The weakly temperature dependent contribution is necessary to account for the non-linear increase in $\bar{\tau}^{-1}$ with temperature at the low temperature end of the curve. The strongly temperature-dependent dipolar contribution indicates that the OEC in state S_0 contains a paramagnetic species which couples strongly to D^+ and is different from the $S = \frac{1}{2}$ binuclear cluster of the S_2-state. The temperature 'resonance' indicates that it is a much faster relaxer than the S_2-state cluster. If we assume that the 'resonance' arises for $\omega T_{1,Mn} = 1$ in Eqn. B-1 of Appendix B, then we are allowed to set $(1/T_1)_d = a'T + 13b/10\omega$, where b is the prefactor in Eqn. 1. From the numerical values for the fit in Fig. 5B, we can then estimate the distance, R, between the Mn and D^+: $R = 28.6$ Å for $S = 1/2$. This value is rather insensitive to the value taken for S, since it is proportional to $[S(S+1)]^{1/6}$ (Eqn. 1): for $S = 5/2$, $R = 43$ Å.

A distance of 30–40 Å between the OEC and the tyrosyl radical seems entirely reasonable. According to Yeates et al. [53], the bacterial reaction center complex at the level of the special pair is a cylinder with a diameter of about 70 Å. Innes and Brudvig found that D^+ is burried $\geqq 25$ Å into the membrane [54]. This agrees with our observation that the redox state of the OEC has no measurable influence on the linewidth and lineshape of Signal II. The Mn's are probably located in the extrinsic loops of the D_1 and D_2 subunits (which have no counterparts in the bacterial reaction center).

The 4-flash sample is predominantly in the S_1-state. Its relaxation vs. temperature curve is much like that of the 0-flash sample, with a small enhancement at 20 K, which is due to the presence of 25% S_0-state (Table I).

A model for the OEC

The main results of the present work are: (i) a strong increase in average relaxation time $\bar{\tau}$ for the $S_0 \rightarrow S_1$ transition; (ii) a decrease in $\bar{\tau}$ (enhancement of average relaxation rate) for the $S_1 \rightarrow S_2$ transition; (iii) little or no change in relaxation for the $S_2 \rightarrow S_3$ transition; and (iv) a further decrease in $\bar{\tau}$ for the $S_3 \rightarrow S_0$ transition. In the following we will discuss a model for the OEC that rationalizes most of the data obtained with spectroscopic techniques: UV absorption, EXAFS and XAES, EPR, and NMR.

First, we have to comment on the relaxation properties of Mn ions [44,46,52,55]. The electronic configuration of Mn^{2+}, Mn^{3+} and Mn^{4+} is $3d^5$, $3d^4$ and $3d^3$, respectively.

$3d^5$-states have an orbital singlet ground state, $^6S_{5/2}$. The next higher orbital state is an excited state that is energetically well separated from the ground state, so that the spin-orbit interaction is small, and relaxation slow. In solution Mn^{2+} is in an hexaquo, octahedral environment, the $\mp\frac{5}{2} \rightarrow \mp\frac{3}{2}$ transitions are broadened because of the anisotropic spin-orbit coupling and only the $+\frac{1}{2} \rightarrow -\frac{1}{2}$ transition is observable. This gives rise to six about equally intense lines, spaced by the hyperfine interaction with the $I = \frac{5}{2}$ nuclear spin of Mn. In the solid state, however, it is likely that the ligand field has much lower symmetry. For example, a tetragonal distortion gives rise to strongly anisotropic transitions, and consequently a very broad EPR line, which may well be unobservable. T_1 of Mn^{2+} in various environments is about 10^{-8} s at 300 K and about 10^{-3} s at 5 K [44].

Mn^{3+} has a $^5D_0$ ground state which for a free ion is orbitally 5-fold degenerate. In an octahedral or tetrahedral ligand field, it is split in a doublet and triplet and by a tetragonal distortion further split to an orbitally singlet ground state. Depending on the strength of the ligand fields, the four d electrons may give rise to a high ($S = 2$) or low ($S = 0$) spin configuration. The nearness of higher orbital states gives rise to strong spin-orbit

coupling and fast relaxation for $S \neq 0$. The $S = 0$ state is diamagnetic and cannot enhance relaxation. The EPR signal of the $S = 2$ state will be strongly anisotropic and in randomly oriented samples difficult to detect.

Mn^{4+} as a free ion has a $^4F_{3/2}$ 7-fold degenerate orbital ground state, which for the bound ion is split by a ligand field. For sufficiently low symmetry, the ground state is again orbitally non-degenerate and the total spin is $S = \frac{1}{2}$, 1 or $\frac{3}{2}$. Hence, it is always magnetic and will generally be an even stronger relaxer than the Mn^{3+} ion because of the strong spin-orbit coupling (many closely lying orbital states). Again, in a randomly oriented sample the EPR signal will be broad and difficult to detect.

We now consider the oxidation state of the four Mn of the OEC in the various S-states. It is most convenient to start with the S_1-state. As argued above, the bi-exponential relaxation can be explained by two separate, magnetically non-coupled Mn centers with different relaxation enhancement and distance to D^+. As discussed earlier, they are expected to be either Mn^{2+} and Mn^{3+} or Mn^{3+} and Mn^{4+}. The question now comes to the assignment of the oxidation state of the two other Mn ions in S_1. Oxidizing S_1 to S_2 enhances the relaxation of D^+, mostly by speeding up the slow component (Table II and III). This is explained most naturally by the formation of the $S = \frac{1}{2}$ spin-coupled pair $Mn^{3+} \cdot Mn^{4+}$ that gives rise to the multiline signal. This pair, which is tightly coupled, cannot give rise to bi-exponential relaxation and it is likely that this is instead caused by the two other Mn ions in the OEC. If this explanation is valid, it is reasonable to suggest that the Mn ions that in S_2 give rise to the multiline signal, in S_1 form a diamagnetic pair with $S = 0$, e.g., a $Mn^{3+} \cdot Mn^{3+}$ pair. This interpretation is analogous to that reached earlier from cw power saturation data [32] and with NMR [21].

Further oxidation to S_3 does not significantly change the relaxation, yet the multiline signal disappears. The most straightforward explanation is that the oxidation state of the Mn cluster does not change, but that the multiline EPR signal is rendered unobservable because of weak interaction of the binuclear $S = \frac{1}{2}$ Mn cluster with a third paramagnet [32]. Such interaction would lead to additional hyperfine splittings, thereby broadening the hyperfine lines without affecting the energy between the spin multiplets, leaving the relaxation properties unchanged. This interpretation is supported by the X-ray spectroscopy (XAES) results [18–20] where no change in oxidation state of the Mn is found, and the proton NMR relaxation measurements [21] where no change in bulk proton relaxation in the $S_2 \rightarrow S_3$ transition is found.

Oxidizing S_3 to S_4 and subsequent reduction to S_0 further enhances the relaxation, mostly because the amplitudes of the fast component increase. This transition almost certainly involves reduction of the Mn cluster. If we assume that the coupled binuclear cluster accepts three electrons, we would again have a mixed valence cluster in the S_0-state, now a $Mn^{2+} \cdot Mn^{3+}$ pair. This conclusion is supported by the NMR data [21]. If the coupling remains antiferromagnetic (and it is difficult to envisage a reversal of the sign of coupling just because of oxidation) then one would expect a $S = \frac{1}{2}$ multiline signal. This is not observed, probably because it is a rather fast relaxer with broad hyperfine lines. Pure S_0 samples are difficult to prepare and the sample used in this study and in [32] was of fairly low concentration (about 10 μM PS II), so that a broadened multiline signal may well have escaped detection.

The dramatic slowing down of the relaxation on the $S_0 \rightarrow S_1$ transition is most naturally explained by oxidation of the binuclear $Mn^{2+} \cdot Mn^{3+}$ cluster to a $S = 0$ $Mn^{3+} \cdot Mn^{3+}$ cluster.

From the above argumentation it follows that the two non-magnetically coupled Mn ions are not oxidized during the $S_0 \rightarrow S_1 \rightarrow S_2 \rightarrow S_3$ sequence. Their oxidation state is either Mn^{3+} (fast relaxing) and Mn^{2+} (non-relaxing) or Mn^{4+} and Mn^{3+}, with the relative relaxing effect on D^+ determined by their ligand field environment and the distance to D^+. EXAFS results yield two distances between the Mn ions of the OEC, 2.7 and 3.3 Å, with likely one Mn 3.3 Å removed from three Mn that have interdistances of 2.7 Å ([18–20] and R. Prince, private communication). The ratio between the relaxation enhancement of two Mn ions $3.3 + 2.7 = 6.0$ Å apart would, for equal S values and correlation times, be 0.33 and 0.43 for a distance between the Mn cluster and D^+ of 30 and 40 Å, respectively (Eqn. 1). Taking into account that the two Mn will differ in S value and τ_c, this is consistent with the observed ratio $\tau_1/\tau_2 =$ 0.12–0.19 (Table II). We note that the results of X-ray spectroscopy favour all Mn to be in a 3^+ or higher oxidation state in the S_1–S_3 states [20], which would suggest that they are Mn^{3+} and Mn^{4+}, as they do not change valence in the oxidation cycle. EPR signals of the single Mn ions in a 3^+ or 4^+ oxidation state will be very broad and difficult to detect. In the $S_3 \rightarrow S_4$ transition one of the strongly bound Mn may be oxidized and function in the concerted water oxidation reaction but at present there is no experimental evidence for this.

The above interpretation agrees partly with the results of UV spectroscopy. The $S_1 \rightarrow S_2$ and $S_2 \rightarrow S_3$ transitions give rise to similar contributions to the UV absorbance changes, which have been interpreted to result from a $Mn^{3+} \rightarrow Mn^{4+}$ oxidation [12–17]. For the $S_1 \rightarrow S_2$ transition this agrees with the present work and the cw EPR results [32], but for the $S_2 \rightarrow S_3$ transition it contrasts with our view, supported by the NMR and XAES results [18–21], that the Mn oxidation state does not change during this transition. The $S_0 \rightarrow S_1$ transition appears to be spectrally different from the $S_1 \rightarrow S_2$ and the $S_2 \rightarrow S_3$ transitions and can be interpreted as a

$Mn^{2+} \rightarrow Mn^{3+}$ oxidation [16,17], in agreement with the NMR and EPR results (Refs. 21 and 32, and this work). We have at present no explanation for the differences in interpretation other than that it is difficult to assign the flash-induced UV absorbance changes to oxidation of a particular species.

We finally compare the results of our relaxation study with the NMR proton relaxation studies of Srinivasan and Sharp [21]. In their work a slight spin-lattice relaxation enhancement of about 1% was found for the $S_1 \rightarrow S_2$ transition and for the formation of S_0 from S_1. We find similarly that the EPR relaxation of D^+ is enhanced for the $S_1 \rightarrow S_2$ transition and de-enhanced for the $S_0 \rightarrow S_1$ transition. At first sight this agreement is puzzling since it is generally held that a good NMR relaxer is a bad EPR relaxer and vice versa. This is because the frequency ω in Eqn. 1 is a factor of about 2000 higher for the EPR than for the NMR experiments, when carried out in the same magnetic field. Thus, the condition $\omega\tau_c \approx 1$ then cannot be simultaneously met for protons and electrons. One has to be careful, however, to apply this reasoning to NMR and EPR experiments carried out at different magnetic fields and quite different temperatures. We will show below that the same relaxer can be responsible for the NMR as well as the EPR relaxation enhancements.

As already stated in the beginning of this section, high-spin Mn^{2+} is the slowest relaxing Mn ion, with relaxation time $T_1 \sim 10^{-8}$ s at 300 K. Thus, for protons resonating at $\omega_p = 2\pi\nu_p = 2\pi \cdot 20$ MHz $\approx 10^8$ s^{-1} at 300 K, $\omega_p \leq (T_{1,Mn})^{-1}$ and we are in the left branch of the curve in Fig. 1 for any Mn ion. For electrons at 5 K resonating at $\omega_e = 2\pi \cdot 9$ GHz $\approx 5 \cdot 10^{10}$ s^{-1}, $\omega_e \gg (T_{1,Mn})^{-1}$ for Mn^{2+} or similar slowly relaxing Mn ions and we are in the right branch of the curve in Fig. 1. The dipolar contributions to the relaxation can then be written:

$$\left(\frac{1}{T_{1p}}\right)_d = B \cdot T_{1,Mn} \quad \text{for protons at 300 K} \tag{7a}$$

$$\left(\frac{1}{T_{1e}}\right)_d = B'/\omega_e^2 T_{1,Mn} \quad \text{for electrons at 5 K} \tag{7b}$$

where B and B' are proportionality factors whose ratio is given by:

$$\frac{B'}{B} = \left(\frac{R_p}{R_e}\right)^6 \cdot \left(\frac{\gamma_e}{\gamma_p}\right)^2 \approx \left(\frac{R_p}{R_e}\right)^6 \cdot (4 \cdot 10^4) \tag{8}$$

R_p and R_e are the distances between the Mn cluster of the OEC and bulk water protons and D^+, respectively. For practical purposes we may take $(1/T_{1p})_d \sim 10^{-2}$ s^{-1} and $(1/T_{1e})_d \sim 50$ s^{-1}. From Eqns. 7a and b it then follows that $B'/B = 50 \cdot \omega_e^2 \cdot T_{1,Mn}$ (5 K) $\cdot 10^2$ $T_{1,Mn}$ (300 K) $\approx 10^{12}$ when we take $T_{1,Mn}$ (5 K) $= 10^6 \cdot T_{1,Mn}$ (300 K) and $T_{1,Mn}$ (300 K) $= 10^{-9}$ s. Note that for a temperature-activated Orbach process we may neglect the field dependence of $T_{1,Mn}$ [44]. Comparing the experimental value of B'/B with that given by Eqn. 8 we see that they agree for $R_p/R_e \approx 17$. This is not an unreasonable value in view of the fact that the proton relaxation may operate through spin diffusion across a fairly large complex of proteins and a lipid membrane phase [21].

Srinivasan and Sharp attributed the relaxation enhancement at the $S_1 \rightarrow S_2$ transitions to a $Mn^{3+} \rightarrow Mn^{4+}$ oxidation, since at 300 K high spin Mn^{4+} often has a much slower relaxation time (and is therefore a better NMR relaxer) than Mn^{3+}. However, in this case the postulated Mn^{3+} oxidation occurs in a strongly coupled binuclear cluster, which at 300 K almost certainly has a much faster relaxation than Mn^{4+} complexes in solution [53]. We prefer therefore to attribute the proton relaxation enhancement to the formation of a $S = \frac{1}{2}$ Mn cluster from a diamagnetic Mn cluster. As we have argued above the diamagnetic cluster is probably $Mn^{3+} \cdot Mn^{3+}$ but this does not follow directly from the NMR result. The fast relaxation of the $Mn^{3+} \cdot Mn^{4+}$ cluster could explain the small proton relaxation enhancement factor, which is much smaller than for simple solutions of paramagnetic Mn^{2+} or Mn^{4+} complexes.

Summarizing our model: (i) Two of the four Mn ions of the OEC form a binuclear, antiferromagnetically coupled cluster. We propose that these ions are in S_0 ($Mn^{2+} \cdot Mn^{3+}$, $S = \frac{1}{2}$), in S_1 ($Mn^{3+} \cdot Mn^{3+}$, $S = 0$), in S_2 ($Mn^{3+} \cdot Mn^{4+}$, $S = \frac{1}{2}$), in S_3 ($Mn^{3+} \cdot Mn^{4+}$, $S = \frac{1}{2}$). This interpretation is in agreement with cw EPR [32], NMR [21] and X-ray spectroscopy [18–20] data. (ii) Two Mn of the OEC are close to D^+ but at different distances. One is a stronger relaxer of D^+ than the other. Their oxidation state differs by one unit, does not change during the $S_0 \rightarrow S_1 \rightarrow S_2 \rightarrow S_3$ sequence, and is either $Mn^{2+} \cdot Mn^{3+}$ or $Mn^{3+} \cdot Mn^{4+}$. X-ray spectroscopy results favour the latter state. We postulate that at higher temperatures there is a charge resonance between the two Mn that is frozen in when cooling to cryogenic temperatures. The interaction between the two Mn giving rise to charge resonance is too weak to provide efficient magnetic coupling.

Acknowledgements

We are indebted to Dr. L.G. Franzén, University of Göteborg, Sweden for a gift of the PS II-enriched membranes. The work carried out in Leiden was supported by the Netherlands Foundation for Chemical Research (SON), financed by the Netherlands Organization for Scientific Research (NWO). S.S. was supported by a long-term post-doctoral grant for biotechnological basic research from Knut and Alice Wallenbergs Foundation, Stockholm, Sweden. A.W.R. was supported by the CNRS.

Appendix A. Decomposition of saturation recovery traces

The saturation recovery trace of each S_j-state can be represented by:

$$f_j(t) = 1 - \sum_i c_{ij}\, e^{-t/\tau_{ij}}, \quad \sum_i c_{ij} = 1 \tag{A-1}$$

The 'area' I_j defined by the recovery trace of the jth pure S-state is given by:

$$I_j = \int_0^\infty 1 - f_j(t)\, dt = \int_0^\infty \sum_i c_{ij}\, e^{-t/\tau_{ij}}\, dt = -\sum_i c_{ij}\tau_{ij} = -\bar{\tau}_j \tag{A-2}$$

The recovery trace of a mixture of S-states is written:

$$F(t) = \sum_j c_j f_j(t) = \sum_j c_j - \sum_j c_j \sum_i c_{ij}\, e^{-t/\tau_{ij}}$$

$$= 1 - \sum_j \sum_i c_j c_{ij}\, e^{-t/\tau_{ij}} \tag{A-3}$$

with $\Sigma_j c_j = 1$ and $j = 0$–4.

The area between the recovery trace and its asymptote for $t \to \infty$ (the shaded area in Fig. 3a) is given by:

$$I = \int_0^\infty 1 - F(t)\, dt = \int_0^\infty \sum_j \sum_i c_j c_{ij}\, e^{-t/\tau_{ij}}\, dt$$

$$= \sum_j c_j \int_0^\infty \sum_i c_{ij}\, e^{-t/\tau_{ij}}\, dt = -\sum_j c_j \bar{\tau}_j = -\bar{\tau} \tag{A-4}$$

Thus, the measured value $\bar{\tau}$ can be decomposed into the individual weight-averaged $\bar{\tau}_j$ for each S_j state:

$$\bar{\tau} = \sum_j c_j \bar{\tau}_j \tag{A-5}$$

Obviously, if only one S-state is present as in the 0-flash sample, $\bar{\tau}$ directly gives the $\bar{\tau}_j$ of that particular S-state. Starting from the 0-flash sample (100% S_1-state), the $\bar{\tau}_j$ values for the S_2, S_3 and S_0 states can be calculated by recursion from the measured $\bar{\tau}$ values of the 0–3-flash sample, using for the c_j values the S-state distributions of Table I. With the $\bar{\tau}_j$ values so obtained, the τ values of the 4- and 5-flash samples can be predicted.

The individual τ_{ij} and c_{ij} of each S_j-state cannot similarly be calculated from the fits for the 0–3 flash sample, because a sum of exponentials is not by itself an exponential. In other words, except for the 0-flash sample, the two exponentials characterized by τ_f and τ_s of the fit to the saturation recovery curves represent averages of more than one exponential, and thus only approximately characterize the true, multi-exponential recovery function. One may show, however, that to first approximation a relation similar to Eqn. (A-5) holds for both τ_f and τ_s:

From Eqn. (A-3) it follows that $F(t)$ can be written:

$$F(t) = 1 - \sum_j c_j c_{1j}\, e^{-t/\tau_{1j}} - \sum_j c_j c_{2j}\, e^{-t/\tau_{2j}} - \ldots \tag{A-6}$$

Expanding the exponentials and retaining only the first two terms one obtains:

$$F(t) \approx 1 - \sum_j c_j c_{1j}(1 - t/\tau_{1j}) - \sum_j c_j c_{2j}(1 - t/\tau_{2j}) - \ldots$$

$$= 1 - \sum_i \left(\sum_j c_j c_{ij} - \sum_j c_j c_{ij} t/\tau_{ij} \right) \tag{A-7}$$

On the other hand, the fit $F(t)^*$ is by definition a sum of exponentials,

$$F(t)^* = 1 - \sum_k a_k\, e^{-t/\tau_k} \approx 1 - \sum_k (a_k - a_k t/\tau_k) \tag{A-8}$$

Equating the terms of the series of Eqns. (A-7) and (A-8) we obtain:

$$a_k = \sum_j c_j c_{kj} \tag{A-9}$$

$$a_k/\tau_k = \sum_j c_j c_{kj}/\tau_{kj} \tag{A-10}$$

Starting with the 0-flash, 100% S_1-sample, the coefficients c_{kj} and the characteristic times τ_{kj} can be derived for each pure S_j-state by recursion from the fits to the recovery traces for the 0–3-flash samples. As a control, the fit values for the 4- and 5-flash sample can then be predicted. Reasonable agreement then provides a justification for the approximation involved in Eqns. (A-7) and (A-8). It will be recognized that the above approximate method to determine c_{kj}, τ_{kj} works best if the experimental τ_k values differ appreciably. Fortunately, for the present work this was always the case.

Appendix B

Temperature dependence of the relaxation of D^+

For simplicity we assume that there is only one relaxer. Extension to more relaxers is straightforward. The temperature dependence of D^+ is then given by Eqns. 1–4 and 5b:

$$\left(\frac{1}{T_1}\right)_{D^+} = a'T + b\left(\frac{T_{1,Mn}}{1 + \omega^2 (T_{1,Mn})^2} + \frac{4T_{1,Mn}}{1 + 4\omega^2 (T_{1,Mn})^2} \right) \tag{B-1}$$

$$\frac{1}{T_{1,Mn}} = B\left(\frac{\tau_v}{1 + \omega^2\tau_v^2} + \frac{4\tau_v}{1 + 4\omega^2\tau_v^2} \right) \tag{B-2}$$

$$\tau_v = \tau_v^0\, e^{(E_v/kT)} \tag{B-3}$$

We may first distinguish two limiting cases for τ_v:

(1) $\omega\tau_v \gg 1$. Then

$$T_{1,Mn} = \frac{\omega^2}{2B}\tau_v = \tau_0'\, e^{E_v/kT} \tag{B-4}$$

(2) $\omega\tau \ll 1$. Then

$$T_{1,Mn} = \frac{1}{5B\tau_v} = \tau_0'' \, e^{-E_v/kT} \tag{B-5}$$

Substituting Eqns. B-4 and B-5 into Eqn. B-1 results in:
(a) $\omega T_{1,Mn} \gg 1$. Then using Eqn. B-4:

$$\text{(a1)} \quad \left(\frac{1}{T_1}\right)_{D^+} = a'T + \frac{2b}{\omega^2 T_{1,Mn}} = a'T + c_1 \, e^{-E_v/kT} \tag{B-6}$$

with $c_1 = 4b\ B/\omega^4\tau_v^0$, and using Eqn. B-5:

$$\text{(a2)} \quad \left(\frac{1}{T_1}\right)_{D^+} = a'T + c_2 \, e^{+E_v/kT} \tag{B-7}$$

with $c_2 = 10b\ B\tau_v^0/\omega^2$
(b) $\omega T_{1,Mn} \ll 1$. Then using Eqn. B-4:

$$\text{(b1)} \quad \left(\frac{1}{T_1}\right)_{D^+} = a'T + 5bT_{1,Mn} = a'T + c_1' \, e^{+E_v/kT} \tag{B-8}$$

with $c_1' = (5b\omega^2/2B)\tau_v^0$, and using Eqn. B-5:

$$\text{(b2)} \quad \left(\frac{1}{T_1}\right)_{D^+} = a'T + c_2' \, e^{-E_v/kT} \tag{B-9}$$

with $c_2' = b/B\tau_v^0$

From Eqns. B-6–B-9 it is seen that there are two functional forms of the temperature dependence of D^+ in the four limiting cases:

$$\text{I.} \quad \left(\frac{1}{T_1}\right)_{D^+} = a'T + c\, e^{+E_v/kT} \tag{B-10a}$$

$$\text{II.} \quad \left(\frac{1}{T_1}\right)_{D^+} = a'T + c\, e^{-E_v/kT} \tag{B-10b}$$

where c is a constant depending on the absolute and relative values of b, B, ω and τ_v^0.

Eqns. (B-10a and b) are plotted in Fig. B1. Note that the curves represent limiting cases, and that via the temperature dependence of τ_v and consequently of $T_{1,Mn}$, one switches from one limiting case to another when varying the temperature. Yet the curves are useful for noting that (i) even strong dipolar interaction may not, or negligibly enhance the relaxation of D^+, (ii) the dipolar contribution always increases the relaxation of D^+ but, depending on the temperature regime and the relative values of b, B, ω and τ_v^0, this increase shows a strong or a weak dependence on the temperature.

In the transition regimes between the four limiting cases, i.e., for $\omega\tau_v \approx 1$ and/or $\omega T_{1,Mn} \approx 1$, we may observe a 'temperature resonance', in which the relaxation of D^+ varies rapidly with temperature. This is also illustrated in Fig. B1.

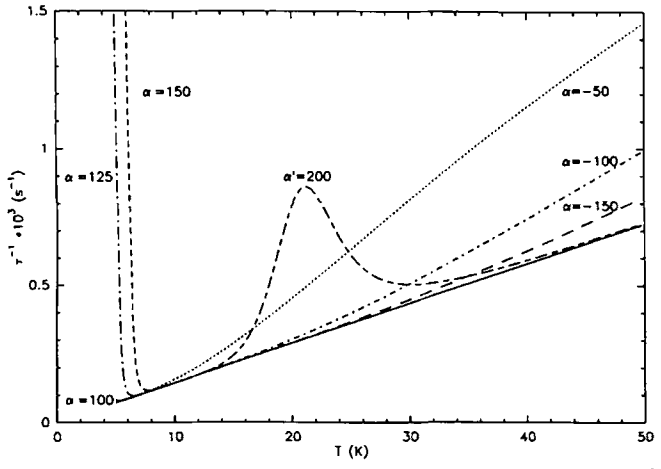

Fig. B1. Some limiting cases of the temperature dependence of $\bar{\tau}^{-1}$ represented by Eqns. B-10a and b. Parameter $\alpha = \pm E_v/k$ (K) as indicated, $a' = 14.5\ K^{-1}\cdot s^{-1}$, $c = 1.95\cdot 10^{13}\ s^{-1}$. The curve labeled $\alpha' = 200$ is obtained by combining Eqn. B-2 and Eqn. B-6 with $2bB/\omega^2 = 1.95\cdot 10^{13}\ s^{-2}$ and $\tau_v = 9\cdot 10^{-16}\ e^{200/T}$ s, $a' = 14.5\ K^{-1}\cdot s^{-1}$.

References

1 Babcock, G.T. (1987) in Photosynthesis (Amesz, J., ed.), Vol. 15, New Comprehensive Biochemistry, pp. 125–158, Elsevier, Amsterdam.
2 Dismukes, G.C. and Siderer, Y. (1981) Proc. Natl. Acad. Sci. USA 78, 274–278.
3 Cooper, S.R., Dismukes, G.C., Klein, M.P. and Calvin, M. (1978) J. Am. Chem. Soc. 100, 7248–7252.
4 Zimmerman, J.L. and Rutherford, A.W. (1984) Biochim. Biophys. Acta 767, 160–167.
5 Hansson, Ö. and Andreasson, L.-E. (1982) Biochim. Biophys. Acta 679, 261–268.
6 Brudvig, G.W., Casey, J.L. and Sauer, K. (1983) Biochim. Biophys. Acta 723, 366–371.
7 Casey, J.L. and Sauer, K. (1984) Biochim. Biophys. Acta 767, 21–28.
8 De Paula, J.C., Beck, W.F. and Brudvig, G.W. (1986) J. Am. Chem. Soc. 108, 4002–4009.
9 Zimmermann, J.L. and Rutherford, A.W. (1986) Biochemistry 25, 4609–4615.
10 Hansson, Ö., Aasa, R. and Vänngård, T. (1987) Biophys. J. 51, 825–832.
11 Dismukes, G.C. and Mathis, P. (1984) FEBS Lett. 178, 51–54.
12 Velthuys, B.R. (1988) Biochim. Biophys. Acta 933, 249–257.
13 Dekker, J.P., Van Gorkom, H.J., Brok, M. and Ouwehand, L. (1984) Biochim. Biophys. Acta 764, 301–309.
14 Dekker, J.P., Van Gorkom, H.J., Wassink, J. and Ouwehand, L. (1984) Biochim. Biophys. Acta 767, 1–9.
15 Plijter, J.J., De Groot, A., Van Dijk, M.A. and Van Gorkom, H.J. (1986) FEBS Lett. 195, 313–318.
16 Lavergne, J. (1987) Biochim. Biophys. Acta 894, 91–107.
17 Saygin, Ö. and Witt, H.T. (1987) Biochim. Biophys. Acta 893, 452–469.
18 Cole, J.L., Yachandra, V.K., McDermotl, A.E., Guiles, R.D., Britt, R.D. and Dexheimer, S.L. (1987) Biochemistry 26, 5967–5773.
19 Yachandra, V.K., Guiles, R.D., McDermott, A.E., Cole, J.L., Britt, R.D., Dexheimer, S.L., Sauer, K. and Klein, M.P. (1987) Biochemistry 26, 5974–5981.
20 Sauer, K., Guiles, R.D., McDermott, A.E., Cole, J.L., Yachandra, V.K., Zimmerman, J.-L., Klein, M.P., Dexheimer, S.L. and Britt, R.D. (1988) Chem. Scr. 28A, 87–91.
21 Srinivasan, A.N. and Sharp, R.R. (1986) Biochim. Biophys. Acta 851, 369–376.
22 Barry, B.A. and Babcock, G.T. (1987) Proc. Natl. Acad. Sci. USA 84, 7099–7103.
23 Debus, R.J., Barry, B.A., Babcock, G.T. and McIntosh, L. (1988) Proc. Natl. Acad. Sci. USA 85, 427–430.

24 Vermaas, W.J.F., Rutherford, A.W. and Hansson, Ö. (1988) Proc. Natl. Acad. Sci. USA 85, 8477–8481.
25 Babcock, G.T. and Sauer, K. (1973) Biochim. Biophys. Acta 325, 504–519.
26 Styring, S. and Rutherford, A.W. (1987) Biochemistry 26, 2401–2405.
27 Velthuys, B.R. and Visser, J.W.M. (1975) FEBS Lett. 55, 109–112.
28 Vermaas, W.F.J., Renger, G. and Dohnt, G. (1984) Biochim. Biophys. Acta 764, 194–202.
29 Warden, J.T., Blankenship, R.E. and Sauer, K. (1976) Biochim. Biophys. Acta 423, 462–478.
30 Yocum, C.F. and Babcock, G.T. (1981) FEBS Lett. 130, 99–102.
31 Yocum, C.F., Yerkes, C.T., Blankenship, R.E., Sharp, R.R. and Babcock, G.T. (1981) Proc. Natl. Acad. Sci. USA 78, 7507–7511.
32 Styring, S. and Rutherford, A.W. (1988) Biochemistry 27, 4915–4293.
33 Nishi, N.N., Hoff, A.J., Schmidt, J. and Van der Waals, J.H. (1978) Chem. Phys. Lett. 58, 164–170.
34 Nishi, N.N., Hoff, A.J. and Van der Waals, J.H. (1980) Biochim. Biophys. Acta 590, 74–88.
35 Britt, R.D., Sauer, K. and Klein, M.P. (1987) in Progress in Photosynthesis Research (Biggins, J., ed.), Vol. 1, pp. 573–576, Martinus Nijhoff Publishers, Dordrecht.
36 De Groot, A., Plijter, J.J., Evelo, R., Babcock, G.T. and Hoff, A.J. (1986) Biochim. Biophys. Acta 848, 8–15.
37 Styring, S. and Rutherford, A.W. (1988) Biochim. Biophys. Acta 933, 378–387.
38 Hoff, A.J., Evelo, R., Styring, S. and Rutherford, A.W. (1987) Rec. Trav. Chim. Pays-Bas 106, 215.
39 Berthold, D.A., Babcock, G.T. and Yocum, C.F. (1981) FEBS Lett. 134, 231–234.
40 Ford, R.C. and Evans, M.C.W. (1983) FEBS Lett. 160, 159–164.
41 Gast, P., Mushlin, R.A. and Hoff, A.J. (1982) J. Phys. Chem. 86, 2886–2891.
42 Solomon, I. (1955) Phys. Rev. 99, 559–565.
43 Bloembergen, N. and Morgan, L.O. (1961) J. Chem. Phys. 34, 842–850.
44 Abragam, A. and Bleany, B. (1970) Electron Paramagnetic Resonance of Transition Ions, Oxford University Press, Oxford.
45 Weger, M. (1960) Bell Syst. Tech. J. 39, 1013–1112.
46 Poole, C.P. and Farach, H.A. (1971) Relaxation in Magnetic Resonance, Academic Press, New York.
47 Salikhov, K.M. and Tsvetkov, Y.D. (1979) in Time Domain Electron Spin Resonance (Kevan, L. and Schwartz, R.N., eds.), pp. 231–277, Wiley Interscience, New York.
48 Lam, E., Baltimore, B., Ortiz, W., Chollar, S., Melis, A. and Malkin, R. (1983) Biochim. Biophys. Acta 724, 201–211.
49 Kuwabara, T. and Murata, N. (1983) Plant Cell Physiol. 24, 741–747.
50 Dismukes, C.G. (1986) Photochem. Photobiol. 43, 99–115.
51 Hsu, B.-D., Lee, J.-Y. and Pan, R.-L. (1987) Biochim. Biophys. acta 890, 89–96.
52 Altschuler, S.A. and Kosyrew, B.M. (1963) Paramagnetische Elektronenresonanz, B.G. Teubner Verlaggesellschaft, Leipzig.
53 Yeates, T.O., Komiya, H., Rees, D.C., Allen, J.B. and Feher, G. (1987) Proc. Natl. Acad. Sci. USA 84, 6438–6442.
54 Innes, J.B. and Brudvig, G.W. (1988) Biophys. J. 53, 614.
55 Lewis, W.B. and Morgan, L.O. (1968) in Transition Metal Chemistry (Carlin, R.L., ed.), Vol. 4, pp. 33–112, Marcel Dekker, New York.